


Enhancing Wireless Transmission from the Body with Wearable Diffractive Patterns

Fengyuan Yang,¹ Pui Mun Lee,¹ Zhenya Dong,¹ Xi Tian,¹ and John S. Ho^{1,2,3,*}

¹*Department of Electrical and Computer Engineering, National University of Singapore, Singapore 117583, Singapore*

²*Institute for Health Innovation and Technology, National University of Singapore, Singapore 117599, Singapore*

³*The N.1 Institute for Health, National University of Singapore, Singapore 117456, Singapore*

 (Received 5 April 2019; revised manuscript received 26 August 2019; published 8 November 2019)

Bioelectronic devices residing within the human body often rely on wireless signals to interact with the external world. The transmission of wireless signals from the body, however, is generally inefficient and energy demanding, in large part due to reflection incurred at the interface between biological tissue and surrounding space. Here, we show that tailored diffractive patterns placed on the surface of the body can enhance wireless transmission by nearly an order of magnitude via the conversion of evanescent waves generated by total internal reflection into propagating waves that transmit into the far field. We develop a theoretical model of this effect at planar interfaces and verify the transmission enhancement numerically and experimentally for nonplanar body surfaces. We then demonstrate clinical utility by increasing the strength of Bluetooth signals received from a wireless device implanted in a large animal model. This enhanced wireless access paves the way for more functional and longer-lasting bioelectronic devices.

DOI: [10.1103/PhysRevApplied.12.054020](https://doi.org/10.1103/PhysRevApplied.12.054020)

I. INTRODUCTION

Bioelectronic devices residing in the human body typically rely on radio-frequency signals in order to wirelessly interact with the external world and perform their diagnostic or therapeutic function. Examples include swallowable endoscopes that transmit images to diagnose gastrointestinal disorders [1–3], artificial pancreas systems that wirelessly coordinate glucose sensors with insulin-delivery pumps [4,5], and spinal-cord stimulators that are wirelessly programmed to mitigate pain [6,7]. A key technological obstacle that must be overcome by such devices is the low efficiency of signal transmission from the human body into the surrounding space. To compensate for this low efficiency, existing wireless systems require transmission at high power levels. State-of-the-art wireless systems operating in the 2.4–2.5-GHz industrial, scientific, and medical band (including Bluetooth and Wi-Fi), for example, transmit at power levels exceeding 1 mW (a pacemaker requires, by comparison, less than 10 μ W [8]), which occupies a significant portion of the power budget for devices such as wireless endoscopes [9], neural recording devices [10], and ingestible sensors [11]. Due to limited available energy resources, these power requirements constrain the overall size, function, and lifetime of wireless devices that operate in the body.

Wireless signals propagating from the human body are attenuated by both tissue absorption and reflection at tissue boundaries. In most clinically relevant configurations, the reflection losses are far more significant than the absorption losses, accounting for more than 80% of the total transmission loss within the radiative 100-MHz to 10-GHz frequency range, because of the large dielectric permittivity of biological tissues (for example, $\epsilon_r = 52.7 + i12.8$ for muscle tissue at 2.45 GHz) [12]. Unlike absorption losses, however, reflection losses can be mitigated because they primarily occur at the interface between the body and its surrounding space. For example, reflection can be circumvented by placing the receiver directly on the surface of the body [13–16] or by submerging the body in an index-matched medium [17–21]. Although used in some imaging applications, these approaches have limited clinical utility because they constrain the range of wireless operation and the mobility of the patient. In principle, reflection can also be eliminated by placing an impedance-matching layer on the surface of the body. The design of such matching layers, however, requires thicknesses on the order of the wavelength, which generally exceeds 10 cm in free space and results in prohibitively bulky and impractical devices.

Here, we demonstrate enhancement of wireless transmission from the body using diffractive patterns placed on the surface of the body [Fig. 1(a)]. The diffractive patterns consist of concentric rings resembling Fresnel zone plates but are patterned at the subwavelength scale and modulate

*johnho@nus.edu.sg

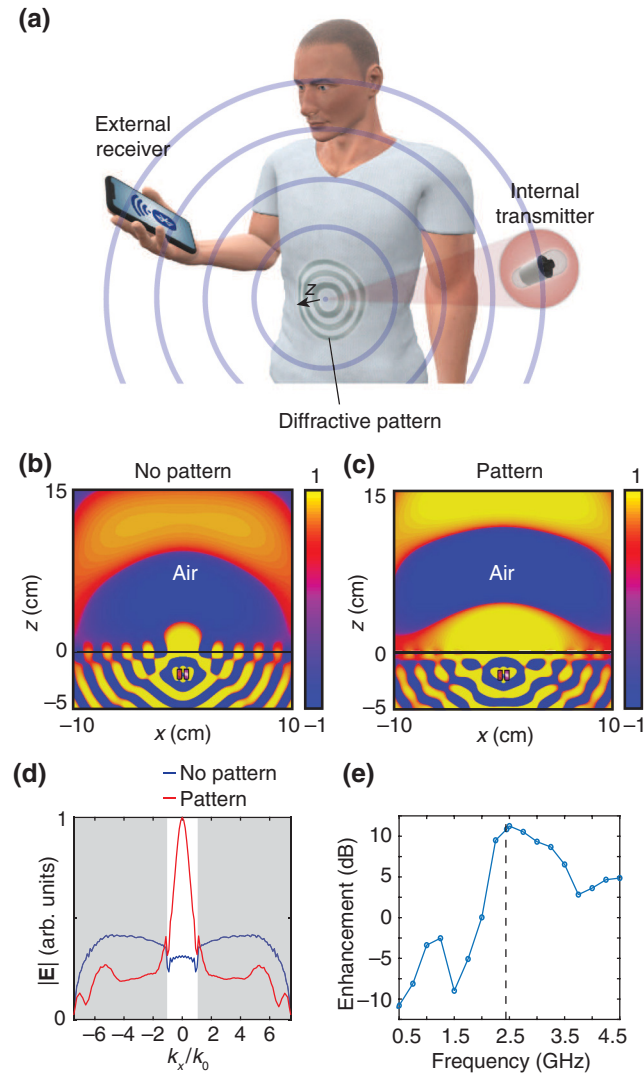


FIG. 1. Enhanced wireless transmission with diffractive patterns. (a) An illustration of wireless transmission from a wireless bioelectronic device inside the body to an external receiver. The surface of the body is modulated with a wearable diffractive pattern. (b),(c) The electric field amplitude (instantaneous) in a planar model of the interface (air $\epsilon_r = 1$ and muscle tissue $\epsilon_r = 52.7$) (b) without and (c) with the diffractive pattern. The source is a dipole 2 cm below the interface oriented in the x direction. (d) The angular spectrum of the electric field on the interface with and without the pattern. The shaded region shows the evanescent-wave components $|k_x| > k_0$. (e) Transmission enhancement as a function of frequency. The operating frequency is 2.45 GHz.

the interface between air and body to convert evanescent waves into propagating waves that transmit into the far field. We develop a theoretical model of transmission through a planar interface that explains this effect and provides design criteria for the diffractive patterns. Using models of the human torso, we numerically and experimentally show that the designed patterns enhance wireless transmission up to an order of magnitude on nonplanar

interfaces. We then demonstrate the utility of this approach in a clinical setting by using diffractive patterns printed on a textile to enhance transmission of Bluetooth signals from within a human-scale porcine model of the body.

II. TRANSMISSION ENHANCEMENT WITH DIFFRACTIVE PATTERNS

Reflection losses encountered at the surface of the body have been estimated in early work using the reflectance of a plane wave at normal incidence to a planar interface $R = |(\epsilon_r^{1/2} - 1)/(\epsilon_r^{1/2} + 1)|^2$, which yields an estimated 58% loss between air and muscle tissue at 2.45 GHz [22]. Recent computational studies, however, show that R significantly underestimates the reflection losses encountered by a wireless signal emitted by a device in the body because it neglects the curvature of the wave front [12]. Due to the localized nature of the source, the wave front is predominantly comprised of wave components incident on the interface at angles larger than the critical angle ($\theta_c \approx 8^\circ$ at the air-muscle interface), which exhibit zero transmission due to total internal reflection, resulting in losses that exceed 80% in most relevant configurations. The conversion of evanescent waves on the surface of the body associated with total internal reflection into propagating waves capable of reaching the far field can therefore enhance wireless transmission without reducing the reflectance R encountered at the normal incidence.

This transmission-enhancement effect is illustrated in Figs. 1(b)–1(e) for a 2.45-GHz dipole source embedded 2 cm deep in the tissue half-space ($\epsilon_r = 52.7$). Finite-difference time-domain simulations of the radiated field show that the field incident on the interface is predominantly evanescent [Fig. 1(b)] and exhibits a transmission of less than 5%. When a diffractive pattern is placed on the surface, however, the transmission across the interface is significantly increased [Fig. 1(c)]. Analysis of the field at the interface shows that the presence of the diffractive pattern results in an angular spectrum that is compressed within the light cone $|k_x| < k_0$ relative to the incident field [Fig. 1(d)], resulting in a total transmission that is increased by about an order of magnitude at the operating frequency [Fig. 1(e)].

A. Theory

We develop a theoretical model that explains this effect for a wireless signal emitted in the tissue half-space. At a large distance r from the interface, the wireless signal in air has a power density $S_\infty(\hat{\mathbf{r}})$, where $\hat{\mathbf{r}}$ is a unit vector pointing into the air half-space taken to be $z > 0$. The efficiency of wireless transmission from the body is given by the following:

$$\eta = \frac{P_t}{P_s} = \frac{1}{P_s} \int_{z>0} d\Omega r^2 S_\infty(\hat{\mathbf{r}}), \quad (1)$$

where P_s is the power emitted by the source, P_t is the power transmitted through the interface into air, and $\int_{z>0} d\Omega$ is the angular integral over the upper hemisphere. The far-field power density $S_\infty(\hat{\mathbf{r}})$ can be expressed in terms of the electric field $\mathbf{E}(\mathbf{r}_s)$ at the interface between air and tissue using the angular-spectrum method. We assume that $\mathbf{E}(\mathbf{r}_s)$ is linearly polarized with phase profile $\phi(\mathbf{r}_s)$ and define the scalar field $F(\mathbf{r}_s) = |\hat{\mathbf{z}} \times \mathbf{E}(\mathbf{r}_s)| e^{i\phi(\mathbf{r}_s)}$. Decomposing the field as $F(\mathbf{r}_s) = \int_{-\infty}^{\infty} d^2k \tilde{F}(\mathbf{k}_s) e^{i\mathbf{k}_s \cdot \mathbf{r}_s}$, we have the following:

$$S_\infty(\hat{\mathbf{r}}) = \left(\frac{2\pi k_0 \hat{r}_z}{c\mu_0 r} \right)^2 |\tilde{F}(k_0 \hat{r}_x, k_0 \hat{r}_y)|^2, \quad (2)$$

where $k_0 = 2\pi/\lambda$ is the wave number in air. Equation (2) shows that the far-field power density depends only on the angular components \mathbf{k}_s within the light cone $|\mathbf{k}_s| < k_0$, which correspond to the radiative components in free space. The angular components of the incident field F_0 outside the cone $|\mathbf{k}_s| > k_0$ do not contribute to far-field transmission because they undergo total internal reflection at the interface. For a dipole source placed in the tissue half-space, the spectrum of the radiated wave lies within the range $|\mathbf{k}_s| < \epsilon_r^{1/2} k_0$. As a result, $\tilde{F}_0(\mathbf{k}_s)$ is mostly evanescent $|\mathbf{k}_s| > k_0$ in the air region [Fig. 1(d)] and incurs much greater reflection losses than predicted by the reflectance at normal incidence.

We now show that modulating the interface with a non-periodic diffractive pattern $D(\mathbf{r}_s)$ can enable the evanescent components to radiate into the far field. To simplify the analysis, we model the diffraction of the incident field $F_0(\mathbf{r}_s)$ by the pattern using the Kirchhoff approximation

$$F(\mathbf{r}_s) = F_0(\mathbf{r}_s)D(\mathbf{r}_s), \quad (3)$$

where $D(\mathbf{r}_s) = 0$ at positions where the pattern is opaque and $D(\mathbf{r}_s) = 1$ otherwise. Taking the Fourier decomposition of Eq. (3) and substituting into Eq. (2), the far-field transmission $S_\infty(\hat{\mathbf{r}})$ is expressed as a convolution integral between the $\tilde{F}_0(\mathbf{k}_s)$ and $\tilde{D}(\mathbf{k}_s)$. In particular, the transmission in the direction $\hat{\mathbf{z}}$ normal to the interface is given by the following:

$$S_\infty(\hat{\mathbf{z}}) = \left(\frac{2\pi k_0}{c\mu_0 r} \right)^2 \left| \int_{-\infty}^{\infty} d^2k \tilde{F}_0(\mathbf{k}_s) \tilde{D}(-\mathbf{k}_s) \right|^2, \quad (4)$$

which has the form of an inner product between the angular spectrum (including evanescent components) of the incident field \tilde{F}_0 and the diffractive pattern \tilde{D} . This far-field transmission now includes contribution from the evanescent components $|\mathbf{k}_s|/k_0 > 1$ but does not directly imply enhanced transmission, since these contributions may destructively interfere. To enhance transmission in the

$\hat{\mathbf{z}}$ direction, $D(\mathbf{r}_s)$ should be selected such that

$$\left| \int_{-\infty}^{\infty} d^2k \tilde{F}_0(\mathbf{k}_s) \tilde{D}(-\mathbf{k}_s) \right| > |\tilde{F}_0(0, 0)|. \quad (5)$$

Applying the same considerations to each direction $\hat{\mathbf{r}}$, it can be seen that transmission enhancement occurs when the diffraction modifies the spatial spectrum of the incident field such that the total energy contained within the light cone $|\mathbf{k}_s| < k_0$ is increased [Fig. 1(d)].

B. Design of the diffractive pattern

To gain insight on the optimal design of the diffractive pattern, we observe that the far-field transmission in Eq. (4) is maximized when $\tilde{D}(\mathbf{k}_s) \propto \tilde{F}_0^*(-\mathbf{k}_s)$ or, in spatial coordinates, $D(\mathbf{r}_s) \propto F_0^*(\mathbf{r}_s)$. This solution corresponds to the matched spatial filter for the incident wave but is complex valued and cannot be implemented using a binary diffractive pattern [23]. In general, the design of a binary pattern maximizing Eq. (4) does not admit an analytical solution and needs to be solved using numerical optimization. We use a heuristic approach that discretizes the matched-filter

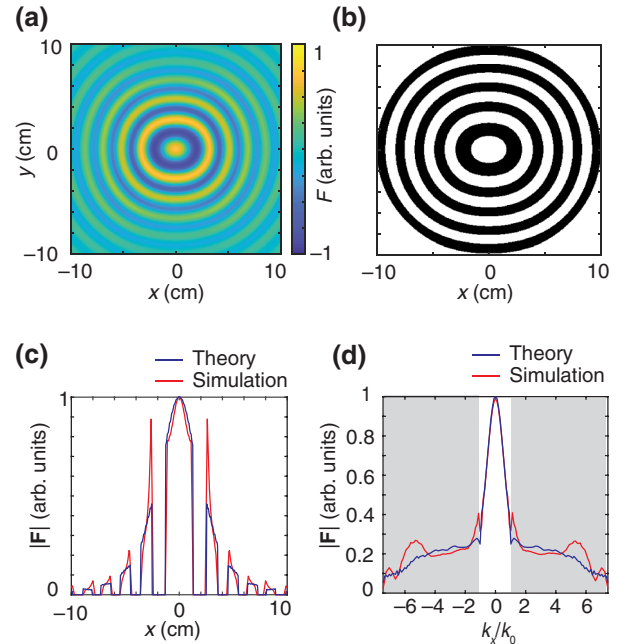


FIG. 2. The modulation of the interface field by the diffractive pattern. (a) The electric field F_0 at the interface generated by a dipole emitter 2 cm deep in tissue. (b) The diffractive pattern D obtained from the phase distribution of the incident field. The black regions indicate areas where $D(\mathbf{r}_s) = 0$ and the white regions where $D(\mathbf{r}_s) = 1$. (c) A comparison of the magnitude of the electric field obtained from the Kirchhoff approximation (theory) and from a numerical solver (simulation) along $y = 0$. (d) The angular spectrum of the corresponding electric field at $y = 0$. The shaded regions show wave components $1 < |k_x/k_0| < 7.3$ that undergo total internal reflection at the interface.

solution using the following rule:

$$D(\mathbf{r}_s) = \begin{cases} 0, & \phi_0(\mathbf{r}_s) \geq \pi, \\ 1, & \phi_0(\mathbf{r}_s) < \pi, \end{cases} \quad (6)$$

where $\phi_0(\mathbf{r}_s)$ is the phase profile of the incident field $F_0(\mathbf{r}_s)$, with the phase reference point taken to be $\phi_0(0) = 0$. Equation (6) can be applied to obtain a diffractive pattern for arbitrarily complex tissue geometries provided that the interfacial field generated by the source can be obtained computationally.

Figures 2(a) and 2(b) show the numerically calculated incident field F_0 and diffractive pattern D obtained using Eq. (6) for the tissue half-space. The diffracted field F predicted by the approximate theory is in close agreement with full-wave simulations of transmission in the presence of the diffractive pattern [Fig. 2(c)]. Consistent with the simulations, the theory shows that the angular spectrum of F lies primarily within the light cone $|\mathbf{k}_s| < k_0$ [Fig. 2(d)]. This compression of the evanescent spectrum of F_0 into the radiation region results in transmission enhancement across the interface. Reminiscent of Fresnel zone plates, the diffractive patterns are ringlike gratings that exploit wave-interference effects. However, unlike Fresnel zone plates and other diffractive devices, the pattern

involves subwavelength spacing between adjacent rings and modulates an incident evanescent field. The function of the diffractive pattern can be understood as a generalized grating coupler that performs surface-to-propagating-wave conversion using a nonperiodic structure that compresses the spectrum of the incident field rather than a periodic structure that provides a fixed-momentum offset.

III. RESULTS

A. Nonplanar surfaces

The diffractive patterns can be unobtrusively placed on the surface of the body by integrating them into clothing or other formats conformal to the body. To demonstrate applicability to nonplanar interfaces, we model the human torso using a cylindrical container (10 cm radius) filled with water to mimic the biological tissue [24]. A dipole transmit antenna is placed in the container 4 cm from the air-water interface and a receive antenna 30 cm (about 2.5λ) away from the interface in the normal direction. The diffractive patterns are fabricated by screen printing stretchable conductive ink (Ag) on textiles (cotton-polyester blend) (see the Appendix). Transmission of power is measured using a vector-network analyzer (VNA), using the scattering parameter $|S_{21}|^2$. Numerical simulations of this

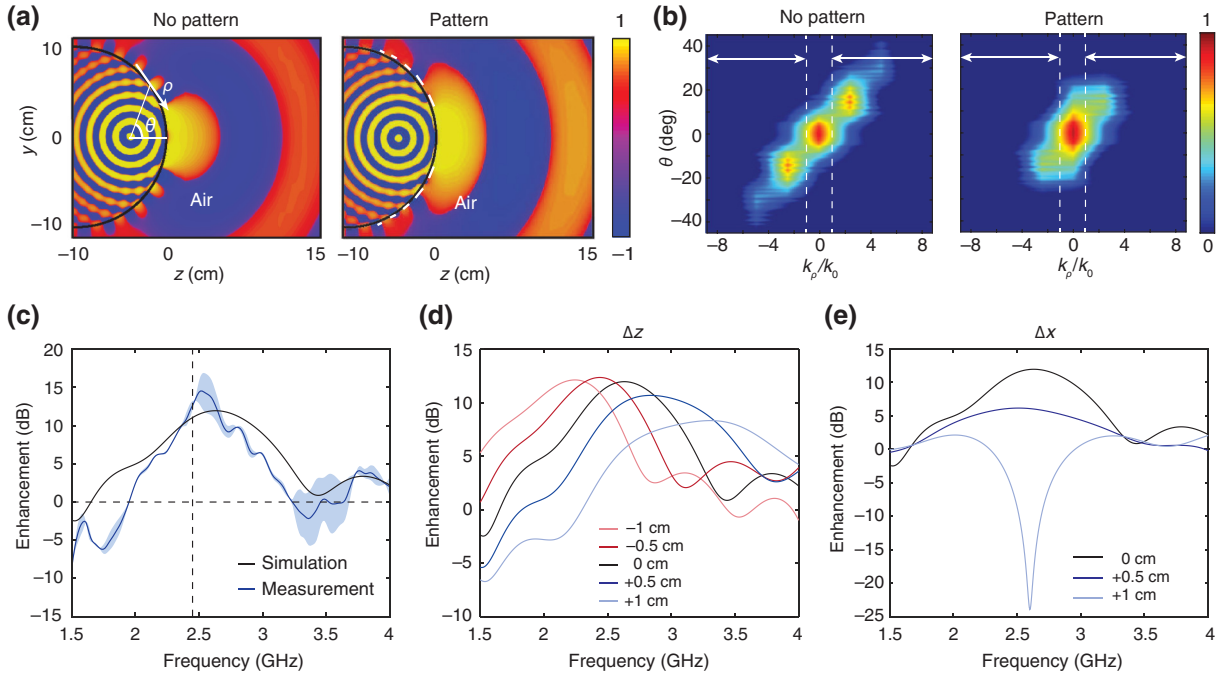


FIG. 3. Transmission enhancement on a curved interface. (a) The simulated electric field amplitude (instantaneous) radiated by a dipole placed 4 cm from the interface in a cylindrical container without and with the diffractive pattern. The dipole is oriented in the x direction. The cylinder is filled with water ($\epsilon_r = 78$ at 2.45 GHz) to model the human torso. (b) The angular spectrum along tangential lines ρ at angle θ from the normal direction without and with the diffractive pattern. The dashed lines and arrows show the region in which $|k_\rho| > k_0$. (c) Simulated and measured transmission enhancement. The measurement graph shows the mean \pm s.d. ($n = 3$ technical trials). (d),(e) Simulated transmission enhancement with varying displacement of the source position in (d) the z direction and (e) the x direction.

configuration show that the mismatch between the curvature of the wave front and the interface results in a strongly reflected incident field (less than 10% transmission) that is a predominantly evanescent field on the interface [Fig. 3(a)]. Placement of the diffractive pattern on the surface based on this incident field results in about 10 dB enhancement of transmission at 2.45 GHz in both simulation and experiment [Fig. 3(c)]. By analyzing the angular spectrum of the simulated field along lines tangential to points on the interface at angle θ from the normal direction, the diffracted field on the interface is found to also exhibit spectral compression [Fig. 3(b)], in which energy in the evanescent region of the spectrum is moved into the propagating region.

As transmission enhancement relies on wave interference, displacing the source by distances compared to a half-wavelength relative to the diffractive pattern can significantly alter transmission behavior. We quantify this effect using simulations for the cylindrical geometry. Figure 3(d) shows that increasing or decreasing the source depth z results in a corresponding rightward or leftward shift in the spectral position of the transmission peak. Lateral displacement in the x direction can result in more pronounced behavior in which 1 cm displacement results in transmission suppression at a specific frequency [Fig. 3(e)]. In both cases, the transmission enhancement is maintained within approximately ± 0.5 cm of the prescribed position at the 2.45-GHz operating frequency.

We next study wireless transmission in an anatomically detailed computational model of the human body. A dipole source is placed 5.5 cm below the abdomen to model transmission from a wireless gastrointestinal device. The radiated field on the surface of the body is shown in Fig. 4(a), with the transverse cutting plane $x = 0$ in plane with the source. The diffractive pattern is designed using the phase profile $\phi_0(\mathbf{r}_s)$ of the incident field, conforming with the nonplanar surface of the body [Fig. 4(b)]. Figures 4(c) and 4(d) show the electric field intensity on the $x = 0$ plane without and with the diffractive pattern. The diffractive pattern enhances wireless transmission by a factor of about 4.5 in this configuration. The far-field radiation pattern shows that the enhancement is strongest in the direction (a factor of 6.3) normal to the interface, although the overall radiation pattern is not significantly changed [Figs. 4(e) and 4(f)].

B. *In situ* demonstration

To demonstrate the clinical feasibility of transmission enhancement, we measure the transmission of wireless Bluetooth signals [25,26] transmitted *in situ* in an adult pig (weight 70 kg) in a radiology room. The experiments are completed within 3 h of euthanasia, such that the tissue properties are expected to be similar to that *in vivo*. We first evaluate wide-band transmission by inserting a

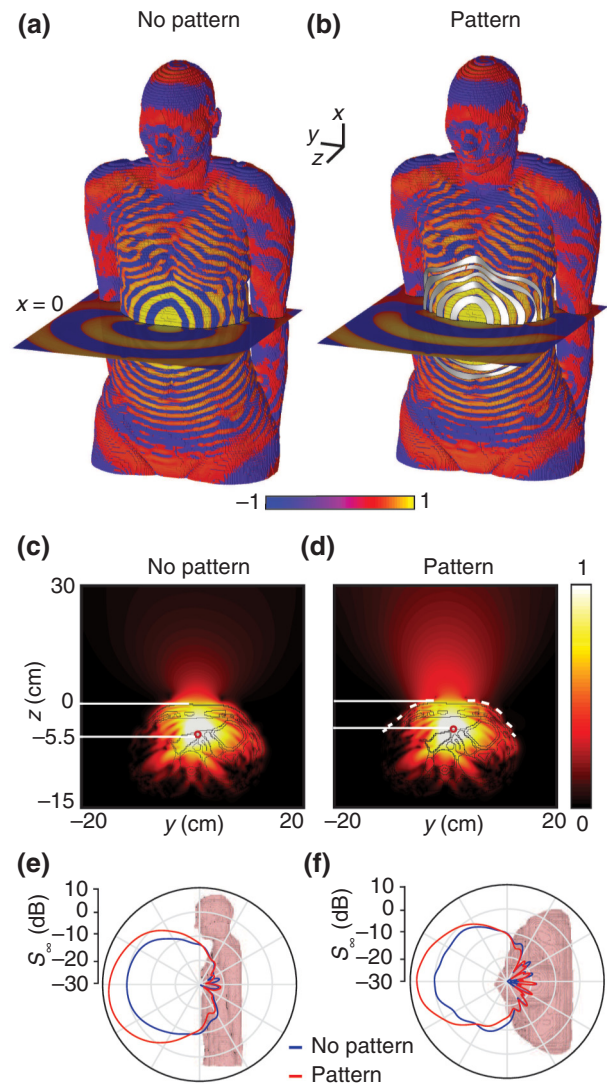


FIG. 4. Transmission enhancement in a computational human body model. (a),(b) The electric field amplitude (instantaneous) radiated by a dipole 5.5 cm deep below the abdomen (a) without and (b) with the diffractive pattern. The transverse cutting plane $x = 0$ is in plane with the source. (c),(d) The electric field intensity (time-averaged) at $x = 0$ (c) without and (d) with the diffractive pattern. (e),(f) The angular distribution of the far-field power density S_∞ without and with the diffractive pattern in the (e) sagittal and (f) transverse planes, normalized to the normal direction \hat{z} without the pattern.

transmit antenna excited by a coaxial cable above the stomach in the euthanized adult pig and measuring S_{21} with a receive antenna positioned 20 cm directly above the abdomen. Computed-tomography imaging shows that the transmitter position is about 5.5 cm below the body surface [Figs. 5(a) and 5(b)]. A wearable diffractive pattern is designed, based on the incident field obtained in the computational human body model, by screen printing the pattern on a textile sheet [Fig. 5(c), see the Appendix]. Placement of the textile on the surface of the body with

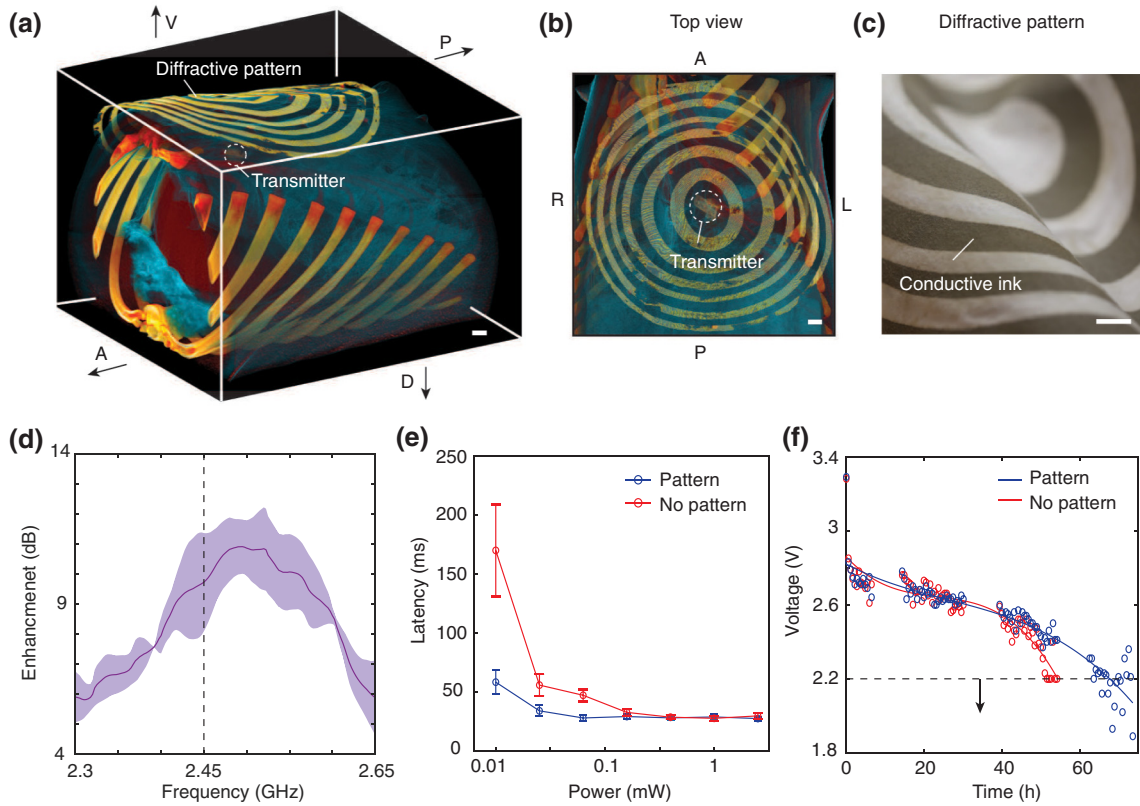


FIG. 5. *In situ* transmission enhancement in a large animal model. (a) The computed-tomography reconstruction of the transmit-device location in the euthanized-adult-pig model. The device is placed above the stomach, about 5.5 cm below the surface of the abdomen. The arrows show the anterior-posterior (A-P) and dorsal-ventral (D-V) directions. (b) A top view of the position of the transmit device aligned with the diffractive pattern. (c) An image of the diffractive pattern printed on a textile. (d) The transmission enhancement measured from a receive antenna placed 20 cm above the abdomen. The graphs show the mean \pm s.d. ($n = 3$ technical trials). (e) The latency of wireless Bluetooth communication as a function of the transmit power with and without a diffractive pattern. The error bars show the mean \pm s.d. ($n = 3$ technical trials). (f) The battery voltage of the wireless module for transmit powers of 0.4 mW (pattern) and 2.5 mW (no pattern). The black dashed line shows the minimum voltage required for stable data transmission. Scale bars: 3 cm.

its center aligned with the transmitter location results in 8 dB enhancement of transmission within the 2.3–2.65-GHz operating-frequency range [Fig. 5(d)].

We next demonstrate enhanced transmission from a completely implanted wireless device comprising a battery-powered Bluetooth module placed in the position of the transmit antenna. The device transmits a wireless signal measured outside of the body using a Bluetooth hub. Figure 5(e) shows the measured Bluetooth transmission latency as a function of the transmit power of the implanted wireless device with and without the diffractive pattern. This latency is related to the signal-to-noise ratio of the received Bluetooth signal in which a lower signal-to-noise ratio results in reduced overall data-transmission rates. At the lowest transmit-power level (0.01 mW), the diffractive pattern reduces the latency by about 70% (equivalent to increasing the transmit power by about 8 dB), which can translate into higher data transfer rates without imposing additional energy requirements on the implanted device.

Alternatively, enhanced transmission enables the transmit power to be lowered without compromising the quality of the wireless communication to achieve longer battery lifetimes. For the Bluetooth module used in this experiment, lowering the transmit power from 2.5 mW to 0.4 mW extends the battery life by 30%, measured by the time required to reach the minimum battery voltage (about 2.2 V) for the wireless function [Fig. 5(f)]. This lifetime can be significantly increased with an optimized design of the wireless device for low-power operation. Notably, the diffractive pattern exhibits a relatively flat dispersion over the wireless-communication bandwidth (2.4–2.5 GHz) and therefore introduces minimal distortion to the communication protocol.

IV. DISCUSSION

We demonstrate that modulating the surface of the body with wearable diffractive patterns can dramatically

enhance the transmission of wireless signals from the body. The key insight underlying this enhancement is that wireless transmission from a localized source is primarily suppressed by total internal reflection—not the impedance mismatch encountered by the normal plane-wave component—and can therefore be enhanced using gratinglike patterns to convert evanescent waves into propagating waves. When enhancing wireless transmission to an external receiver, reciprocity implies that transmission from the external device to the internal device is also enhanced [24]. This enhancement can be understood as a consequence of focusing: the subwavelength features of the diffractive pattern generate the high-wave-vector components necessary to produce a focal spot in the body smaller than the wavelength in air.

Future work should address the robustness of the enhancement effect as well as the role of impedance mismatch. The enhancement effect is currently sensitive to relative displacements exceeding 5 mm. Stretchable or skin-adhesive fabrics can maintain surface placement within this range and the positions of implanted devices within the body are also typically secure at this scale. However, for ingestible, cardiac, and other devices where the position varies significantly, pattern designs that are more robust to displacement may be required. Although the enhancement achieved is significant, diffractive patterns cannot provide reflectionless transmission because they do not resolve the impedance mismatch between biological tissue and air. Recent work on bianisotropic and cascaded metasurfaces [27,28] can enable the realization of arbitrary surface impedances, which may enable impedance-matching layers with deeply subwavelength thicknesses to be realized.

ACKNOWLEDGMENTS

We thank Zac Goh for the artwork used in Fig. 1 and Ruth Yap for assistance on the preparation of the manuscript. This work was supported by a grant from the National Research Foundation, Singapore (Grant No. NRFF2017-07) and the Ministry of Education, Singapore (Grant No. MOE2016-T3-1-004).

APPENDIX

1. Numerical methods and design

Simulations are performed using a commercial finite-difference time-domain solver (CST Microwave Suite). For all the simulations, a miniaturized electric dipole with a length of 1 cm and a cross-section radius of 0.5 cm is used to model the source. Analysis of the electric field at the interface is performed using MATLAB. The diffractive patterns are obtained by obtaining the spatial distribution of the phase $\phi_0(\mathbf{r}_s)$ and thresholding the function $\phi_0(\mathbf{r}_s) > \pi$, using the center point (aligned with the source point) as

the zero phase reference. The dimensions are given in Ref. [24].

2. Experimental methods

The experiments are conducted using a female pig (age 6 months, weight 70 kg) in a radiology room. A transmit antenna (RN-SMA-S-RP, Microchip Technology) is placed inside the abdomen at about 5.5 cm depth. A receive antenna (TG.30.8111, Taoglas) is placed 20 cm above the surface, also aligned with the center of the pattern. Both of these antennas are connected to a portable VNA (Keysight Technologies, FieldFox Handheld Analyzers N9915A). S_{21} is first measured without the diffractive pattern, as a baseline for comparison. Then, a cloth comprising the silver-conductive-ink screen-printed diffractive pattern is placed on the skin of the pig. For each technical trial, the position of the diffractive is adjusted to align the antenna in the center of the pattern through radiological imaging and signal measurements.

Wireless communication is performed using the Bluetooth Low Energy (BLE) protocol. In the pig's abdomen, a single-mode Bluetooth v4.0 module (Laird Technologies, BL600) is implanted 5.5 cm deep under the skin and configured with an integrated antenna, a coin-cell battery adapter (Laird Technologies, BA600), and a 3-V lithium battery (Renata, CR1632). The latency measurements and data transmission are performed using connectivity-testing software (Laird Technologies, UwTerminalX) run from a laptop connected to a hub device (Laird Technologies, BL620). The device is placed 20 cm above the pig's abdomen and wirelessly connected to the implanted Bluetooth module.

3. Diffractive pattern fabrication

The diffractive patterns are fabricated using a conventional screen-printing process using stretchable silver conductive ink (PE873, DuPont). A photo emulsion (Speedball Diazo) is uniformly mixed with a sensitizer in a dark environment and the mixture is spread evenly on the bottom side of a nylon silk screen frame, using a squeegee. The silk screen frame is dried overnight in a dark cabinet. The diffractive pattern is then printed on an OHP transparency film, using an inkjet printer, to form the mask. The mask is then adhered onto the top side of the dried silk-screen frame and photoexposed for 8 min (500-W halogen floodlight (GEWISS GW84215 W.T.) placed 50 cm above the silk screen frame). The silk screen is washed with water, yielding the negative mask. To print the pattern, a cotton shirt is adhered uniformly on the negative-masked silk-screen frame. Conductive silver ink (Dupont PE873) is spread evenly on the patterned area and the shirt is baked on a hot plate (IKA 3581400) at 100 °C for 10 min to ensure that the ink is completely dried and to achieve high conductivity. The conductive area is then coated with

encapsulant (Dupont PE773) and baked on a hot plate at 100 °C for 10 min to provide water and abrasion resistance.

-
- [1] G. Iddan, G. Meron, A. Glukhovsky, and P. Swain, Wireless capsule endoscopy, *Nature* **405**, 417 (2000).
- [2] C. J. Bettinger, Materials advances for next-generation ingestible electronic medical devices, *Trends Biotechnol.* **33**, 575 (2015).
- [3] S. Christoph, A. Alex, N. Phillip, P. C. Anantha, L. Robert, and T. Giovanni, Ingestible electronics for diagnostics and therapy, *Nat. Rev. Mater.* **4**, 83 (2019).
- [4] E. Daniela, D. B. David, and H. Roman, Closed-loop insulin delivery for treatment of type 1 diabetes, *BMC Med.* **9**, 120 (2011).
- [5] L. Parks and T. Y. Kim, Using remote communication technology in insulin pump training: A feasibility study, *J. Diabetes Sci. Technol.* **10**, 398 (2015).
- [6] M. A. Howard III, M. Utz, T. J. Brennan, B. D. Dalm, S. Viljoen, N. D. Jeffery, and G. T. Gillies, Intradural approach to selective stimulation in the spinal cord for treatment of intractable pain: Design principles and wireless protocol, *J. Appl. Phys.* **110**, 044702 (2011).
- [7] N. M. Schuster and A. M. Rapoport, New strategies for the treatment and prevention of primary headache disorders, *Nat. Rev. Neurol.* **12**, 635 (2016).
- [8] L. S. Y. Wong, S. Hossain, A. Ta, J. Edvinsson, D. H. Rivas, and H. Naas, A very low-power CMOS mixed-signal IC for implantable pacemaker applications, *IEEE J. Solid-State Circuits* **39**, 2446 (2004).
- [9] X. Chen, X. Zhang, L. Zhang, X. Li, N. Qi, H. Jiang, and Z. Wang, A wireless capsule endoscope system with low-power controlling and processing ASIC, *IEEE Trans. Biomed. Circuits Syst.* **3**, 11 (2009).
- [10] H. Miranda, V. Gilja, C. A. Chestek, K. V. Shenoy, and T. H. Meng, HermesD: A high-rate long-range wireless transmission system for simultaneous multichannel neural recording applications, *IEEE Trans. Biomed. Circuits Syst.* **4**, 181 (2010).
- [11] K. Kalantar-zadeh, K. J. Berean, N. Ha, A. F. Chrimes, K. Xu, D. Grando, J. Z. Ou, N. Pillai, J. L. Campbell, R. Brkljača, K. M. Taylor, R. E. Burgell, C. K. Yao, S. A. Ward, C. S. McSweeney, J. G. Muir, and P. R. Gibson, A human pilot trial of ingestible electronic capsules capable of sensing different gases in the gut, *Nat. Electron.* **1**, 79 (2018).
- [12] D. Nikolayev, M. Zhadobov, P. Karban, and R. Sauleau, Electromagnetic Radiation Efficiency of Body-Implanted Devices, *Phys. Rev. Appl.* **9**, 024033 (2018).
- [13] E. Y. Chow, Y. Chin Lung, O. Yuehui, A. L. Chlebowski, P. P. Irazoqui, and W. J. Chappell, Wireless powering and the study of rf propagation through ocular tissue for development of implantable sensors, *IEEE Trans. Antennas Propag.* **59**, 2379 (2011).
- [14] D. R. Agrawal, Y. Tanabe, D. Weng, A. Ma, S. Hsu, S. Y. Liao, Z. Zhen, Z. Y. Zhu, C. Sun, Z. Dong, F. Yang, H. F. Tse, A. S. Y. Poon, and J. S. Ho, Conformal phased surfaces for wireless powering of bioelectronic microdevices, *Nat. Biomed. Eng.* **1**, 0043 (2017).
- [15] Z. H. Jiang, D. E. Brocker, P. E. Sieber, and D. H. Werner, A compact, low-profile metasurface-enabled antenna for wearable medical body-area network devices, *IEEE Trans. Antennas Propag.* **62**, 4021 (2014).
- [16] S. J. A. Majerus, P. C. Fletter, M. S. Damaser, and S. L. Garverick, Low-power wireless micromanometer system for acute and chronic bladder-pressure monitoring, *IEEE Trans. Biomed. Eng.* **58**, 763 (2011).
- [17] F. A. Gibbs, M. D. Sapozink, K. S. Gates, and J. R. Stewart, Regional hyperthermia with an annular phased array in the experimental treatment of cancer: Report of work in progress with a technical emphasis, *IEEE Trans. Biomed. Eng.* **31**, 115 (1984).
- [18] E. C. Fear and M. A. Stuchly, Microwave detection of breast cancer, *IEEE Trans. Microw. Theory Techn.* **48**, 1854 (2000).
- [19] M. Klemm, J. A. Leendertz, D. Gibbins, I. J. Craddock, A. Preece, and R. Benjamin, Microwave radar-based differential breast cancer imaging: Imaging in homogeneous breast phantoms and low contrast scenarios, *IEEE Trans. Antennas Propag.* **58**, 2337 (2010).
- [20] C. Franconi, J. Vrba, F. Micali, and F. Pesce, Prospects for radiofrequency hyperthermia applicator research. I—Pre-optimised prototypes of endocavitary applicators with matching interfaces for prostate hyperplasia and cancer treatments, *Int. J. Hyperthermia* **27**, 187 (2011).
- [21] X. He, W. Geyi, and S. Wang, A hexagonal focused array for microwave hyperthermia: Optimal design and experiment, *IEEE Antennas Wireless Propag. Lett.* **15**, 56 (2016).
- [22] N. Kuster and Q. Balzano, Energy absorption mechanism by biological bodies in the near field of dipole antennas above 300 MHz, *IEEE Trans. Veh. Technol.* **41**, 17 (1992).
- [23] J. S. Ho, B. Qiu, Y. Tanabe, A. J. Yeh, S. Fan, and A. S. Y. Poon, Planar immersion lens with metasurfaces, *Phys. Rev. B* **91**, 125145 (2015).
- [24] See the Supplemental Material at <http://link.aps.org/supplemental/10.1103/PhysRevApplied.12.054020> for the experimental methods, analysis of the interfacial field, and the design of the diffractive pattern.
- [25] Y. L. Kong, X. Zou, C. A. McCandler, A. R. Kirtane, S. Ning, J. Zhou, A. Abid, M. Jafari, J. Rogner, D. Minahan, and J. E. Collins, 3D-printed gastric resident electronics, *Adv. Mater. Technol.* **4**, 1800490 (2018).
- [26] H. Qian, P. C. Loizou, and M. F. Dorman, A phone-assistive device based on Bluetooth technology for cochlear implant users, *IEEE Trans. Neural Syst. Rehabil. Eng.* **11**, 282 (2003).
- [27] C. Pfeiffer and A. Grbic, Metamaterial Huygens' Surfaces: Tailoring Wave Fronts with Reflectionless Sheets, *Phys. Rev. Lett.* **110**, 197401 (2013).
- [28] S. A. Tretyakov, Metasurfaces for general transformations of electromagnetic fields, *Philos. Trans. Royal Soc. A* **373**, 20140362 (2015).